Journal of Thermal Analysis and Calorimetry
https://doi.org/10.1007/s10973-020-10481-9

Energy and mass transport of Casson nanofluid flow over a slanted permeable inclined surface

K. Rafique[1] · M. A. Imran[4] · M. I. Anwar[2,3] · M. Misiran[1] · A. Ahmadian[5]

Received: 17 September 2020 / Accepted: 10 December 2020

Abstract
In this problem, examination of Casson nanofluid flow over nonlinear slanted extending sheet with chemical reaction and heat generation/absorption influences are under thought. Nanofluid exhibits in this examination is established on Buongiorno model. The governing nonlinear PDE's are reduced to nonlinear ODE's by employing suitable transformations. The Keller-box numerical technique is considered for simulation of this research. The influence of chemical reaction and nonlinear parameter on concentration and velocity distribution is analyzed. The recovered results exhibit that the impact of inclination and Casson factor reduced liquid velocity. While energy and mass transport rates are increased against inclination factor. Numerical and graphical outcomes are additionally exhibited in tables and graphs.

Keywords Casson nanofluid · Chemical reaction · MHD · Nonlinear · Inclined surface

List of symbols

C	Fluid concentration (kg m^{-3})
C_f	Skin friction coefficient
C_∞	Ambient concentration (kg m^{-3})
C_w	Fluid wall concentration (kg m^{-3})
C_p	Specific heat (JKg^{-1} K^{-1})
D_B	Brownian diffusion coefficient (m^2 s^{-1})
D_T	Thermophoretic diffusion coefficient (m^2 s^{-1})
f	Similarity function for velocity
ρc_p	Volume heat capacity
ϕ	Dimensionless solid volume fraction
Gr	Local Grashof number
σ	Electric conductivity (Sm)
α	Thermal diffusivity
u	Velocity in x direction (m s^{-1})
θ	Dimensionless temperature
ρ	Fluid density (kg m^{-1})
β	Casson parameter
Q_0	Dimensional heat generation or absorption
Le	Lewis number
Nb	Brownian motion parameter
Nt	Thermophoretic parameter
Nu	Nusselt number
Pr	Prandtle number
g	Gravitational acceleration
μ	Dynamic viscosity (Ns m^{-2})
W	Condition at the wall
β_t	Thermal expansion coefficient
ψ	Stream function (m s^{-1})
γ	Inclination parameter
v	Velocity in y direction (m s^{-1})
m	Nonlinear stretching parameter
Gc	Local modified Grashof number
a	Stretching rate (s^{-1})
R	Chemical reaction
Re_x	Reynolds number
Sh	Sherwood number
T	Fluid temperature (K)
T_w	Wall temperature (K)
T_∞	Ambient temperature (K)
u_w	Wall velocity (m s^{-1})
λ_1	Heat generation or absorption parameter
ν	Kinematic viscosity (m^2 s^{-1})

✉ A. Ahmadian
ali.ahmadian@ukm.edu.my

[1] School of Quantitative Sciences, Universiti Utara Malaysia, 06010 Sintok, Kedah, Malaysia

[2] Department of Mathematics, Faculty of Science, University of Sargodha, Sargodha, Pakistan

[3] Higher Education Department (HED) Punjab, Lahore, Pakistan

[4] Department of Mathematics, University of Management and Technology, Lahore, Pakistan

[5] Institute of IR 4.0, The National University of Malaysia, 43600 UKM Bangi, Malaysia

Published online: 06 February 2021

∞	Ambient condition
β_c	Concentration expansion coefficient
M	Hartmann number
f'	Differentiation with respect to η
(x, y)	Cartesian coordinate (m)
k	Thermal conductivity ($Wm^{-1} K^{-1}$)
B_0	Uniform magnetic field (kg s^{-2} A^{-1})
S	Suction or injection parameter

Introduction

Non-Newtonian liquids picked up the fascination of researchers because of its broad assortment of employments in industry and designing. Casson liquid is a standout among the most basic characterizations of non-Newtonian fluids. It is shear diminishing liquid which is recognized to have endlessness viscidness at zero measure of shear and no viscidness on boundless degree of shear and, stress below which no movement take place. Some samples of Casson fluid comprize human blood, broth, rigorous fruit liquids, tomato paste, metallurgy, and jam, etc. Rafique et al. [1] studied behavior of Casson nanofluid flow for slanted surface. Recently, Anwar et al. [2] investigated Casson nanomaterial for permeable surface numerically. For detail literature see references [3–22].

In the past couple of eras, rapid developments in nanotechnology have brief generating of new age coolants called "Nanoliquid." Nanoliquids are potential heat trade fluids with developed thermo physical properties and heat trade performance can be associated in various tools for better exhibitions (for example imperativeness, heat exchange, and other performances).Nanoliquids are organized by snooping with nanoparticles in ordinary heat exchange liquids with typical sizes below 100 nm for example, oil, water, and ethylene glycol. These are ebb and flow heat exchange controllers that activate the thermal conductivity of the base liquids and an important topic for specialists and scientists over the period of the most modern couple of years because of its various development and present-day uses. Eastman et al. [23] inspected in an investigation when nanoparticles are included base liquid (water) with volume portion 5% thermal conductivity upgraded up to 60%. Moreover, Eastman et al. [24] announced that the thermal conductivity expanded up to 40% by including the copper nanoparticles with volume part 1% in the customary liquid ethylene glycol or oil. Buongiorno [25] has talked about in his investigation there are seven systems, which are imperative to upgrade the thermal conductivity of the regular liquid. Among all these Brownian movement and thermophoresis are increasingly significant. Recently, several researchers investigated flow of nanofluid with different effects [26–32].

The heat and mass exchange with chemical reaction over a slanted extending plate have achieved a considerable concentration of researchers because of its various uses in engineering. Chemical reactions divided into single-step or multi-step reactions, and in catalyst or noncatalyst reactions. Mostly, chemical reaction consists on different steps for instance primary steps due to which it becomes complex. In order to reduce this complexity, we require a mathematical model. The mathematical chemistry accomplishes mathematical model of the chemical procedure whereas, computational chemistry utilizes computer performances to reveal the chemical problems. The research of reaction rate and chemical procedure is a significant portion of today's science, to examine the characteristics and structures of atoms and molecules, to switch, enhance, and motivate the process. Today we can discuss the complete reaction mechanism examines the whole collaboration among energy exchange performance and fast reactions in profound insights. For deep knowledge about latest concern research see [33–38].

Above-said literature reveals that no study has been conducted yet for Casson nanofluid for nonlinear slanted surface by incorporating chemical reaction and het generation or absorption. Therefore, here we have presented the numerical simulation to tackle the features of Casson nanofluid flow on slanted sheet by employing Keller-box technique. Further, we can also use another numerical technique for the numerical solution of this problem but Keller-box method is easier to program, more flexible and more friendly as compared with other methods.

Problem formulation

Casson Nanofluid on a porous slanted nonlinear enlarging plate with an angle γ is under account. The stretching and free stream speeds are supposed to stand as, $u_w(x) = ax^m$ and $u_\infty(x) = 0$, respectively, here 'x' is the coordinate dignified along the extending surface by taking 'a' constant. The Brownian motion and thermophoresis properties are taken into account. Suction or injection is under discussion along with chemical reaction and heat generation or absorption (Fig. 1).

The flow equations for this study are given by

$$\frac{\partial u}{\partial x} + \frac{\partial v}{\partial y} = 0 \tag{1}$$

$$u\frac{\partial u}{\partial x} + v\frac{\partial u}{\partial y} = \nu\left(1 + \frac{1}{\beta}\right)\frac{\partial^2 u}{\partial y^2} + g\left[\beta_t(T - T_\infty) + \beta_c(C - C_\infty)\right]\cos\gamma - \left(\frac{\sigma B_0^2}{\rho}\right)u \tag{2}$$

$$u\frac{\partial T}{\partial x}+v\frac{\partial T}{\partial y}=\alpha\frac{\partial^2 T}{\partial y^2}+\tau\left[D_{\mathrm{B}}\frac{\partial C}{\partial y}\frac{\partial T}{\partial y}+\frac{D_{\mathrm{T}}}{T_\infty}\left(\frac{\partial T}{\partial y}\right)^2\right]+\frac{Q_0}{\rho C_{\mathrm{p}}}\left(T-T_\infty\right) \tag{3}$$

$$\psi=\sqrt{\frac{2\nu a x^{\mathrm{m}-1}}{m+1}}f(\eta),\quad \eta=y\sqrt{\frac{(m+1)ax^{\mathrm{m}1}}{2\nu}}\quad .\quad \theta(\eta)=\frac{T-T_\infty}{T_{\mathrm{w}}-T_\infty},\quad \phi(\eta)=\frac{C-C_\infty}{C_{\mathrm{w}}-C_\infty} \tag{7}$$

On substituting Eq. (7), system of Eqs. (2)–(4) reduces to the following nonlinear ordinary differential equations:

$$\left(1+\frac{1}{\beta}\right)f'''+f''f-\left(\frac{2m}{m+1}\right)f'^2+\frac{2}{m+1}\left(Gr_{\mathrm{x}}\theta-Gc_{\mathrm{x}}\phi\right)\cos\gamma-\left(\frac{2M}{m+1}\right)f'=0 \tag{8}$$

$$u\frac{\partial C}{\partial x}+v\frac{\partial C}{\partial y}=D_{\mathrm{B}}\frac{\partial^2 C}{\partial y^2}+\frac{D_{\mathrm{T}}}{T_\infty}\frac{\partial^2 T}{\partial y^2}-R^*\left(C-C_\infty\right) \tag{4}$$

where u and v are the components of velocity in x and y directions, respectively, g is the acceleration due to gravity, B_0 is the uniform magnetic field strength, σ denotes the electrical conductivity, β_{t} is the factor of thermal extension, β_{c} denotes the factor of concentration enlargement, D_{B} denotes the Brownian diffusion factor, and D_{T} denotes the thermophoresis diffusion factor, Q_0 is the heat generation or absorption coefficient, R^* is the chemical reaction coefficient.

The subjected boundary conditions are

$$u=u_{\mathrm{w}}(x)=ax^{\mathrm{m}},\quad v=V_{\mathrm{w}},\quad T=T_{\mathrm{w}},\quad C=C_{\mathrm{w}}\quad \text{at}\quad y=0,\quad u\to 0,\quad v\to 0,\quad T\to T_\infty,\quad C\to C_\infty\quad at\quad y\to\infty, \tag{5}$$

Here we obtained nonlinear ordinary differential equations from nonlinear partial differential equations by using stream function $\psi=\psi(x,y)$ demarcated as

$$u=\frac{\partial\psi}{\partial y},\quad v=-\frac{\partial\psi}{\partial x}. \tag{6}$$

where Equation (1) is fulfilled identically. The similarity transformations are demarcated as

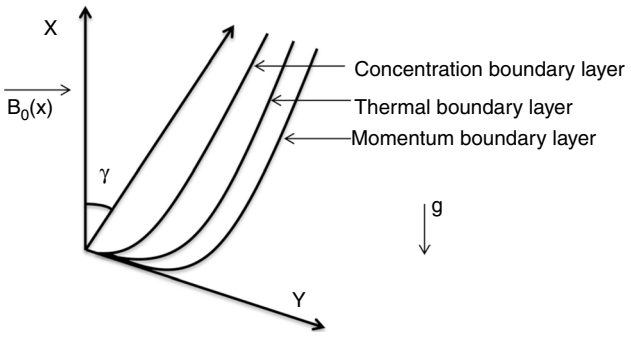

Fig. 1 Physical geometry with coordinate system

$$\left(\frac{1}{\mathrm{Pr}}\right)\theta''+f\theta'+\lambda_1\theta'+Nb\phi'\theta'+Nt\theta'^2=0 \tag{9}$$

$$\phi''+Lef\phi'+Nt_{\mathrm{b}}\theta''-LeR\phi=0 \tag{10}$$

where

$$M=\left(\frac{\sigma B_0^2}{a\rho}\right),\quad Le=\frac{\nu}{D_{\mathrm{B}}},Pr=\frac{\nu}{\alpha},\quad Nb=\frac{\tau D_{\mathrm{B}}\left(C_{\mathrm{w}}-C_\infty\right)}{\nu},\quad Nt=\frac{\tau D_{\mathrm{t}}\left(T_{\mathrm{w}}-T_\infty\right)}{\nu T_\infty},$$
$$Gr_{\mathrm{x}}=\frac{g\beta_{\mathrm{t}}\left(T_{\mathrm{w}}-T_\infty\right)x^{-1}}{a^2},\quad Re_{\mathrm{x}}=\frac{u_{\mathrm{w}}(x)x}{\nu},\quad Gc_{\mathrm{x}}=\frac{g\beta_{\mathrm{c}}\left(C_{\mathrm{w}}-C_\infty\right)x^{-1}}{a^2},$$
$$Nt_{\mathrm{b}}=\frac{N_{\mathrm{t}}}{N_{\mathrm{b}}},\quad \lambda_1=\frac{Q_0}{a\rho c_{\mathrm{p}}},\quad R=\frac{R^*}{a} \tag{11}$$

Here Gr_{x} signifies the local Grashof number, Gc_{x} denotes the local modified Grashof number, Here in order to make local Grashof number and local modified Grashof number free from x, the coefficient of thermal expansion β_{t} and coefficient of concentration expansion β_{c} are proportional to x^1. Hence, we assume that (see references [39, 40])

$$\beta_{\mathrm{t}}=nx^1,\quad \beta_{\mathrm{c}}=n_1x^1 \tag{12}$$

Here n and n_1 are constants, and thus Gr_{x} and Gc_{x} become

$$Gr=\frac{gn\left(T_{\mathrm{w}}-T_\infty\right)}{a^2},\quad Gc=\frac{gn_1\left(C_{\mathrm{w}}-C_\infty\right)}{a^2}.$$

The equivalent boundary settings are converted to

$$f(\eta)=S,\quad f'(\eta)=1,\quad \theta(\eta)=1,\quad \phi(\eta)=1\quad \text{at}\quad \eta=0,\quad f'(\eta)\to 0,\quad \theta(\eta)\to 0,\quad \phi(\eta)\to 0\quad \text{as}\quad \eta\to\infty, \tag{13}$$

The skin friction, Sherwood number, and Nusselt number for the current study are defined as

$$Nu_{\mathrm{x}}=\frac{xq_{\mathrm{w}}}{k\left(T_{\mathrm{w}}-T_\infty\right)},\quad Sh_{\mathrm{x}}=\frac{xq_{\mathrm{m}}}{D_{\mathrm{B}}\left(C_{\mathrm{w}}-C_\infty\right)},\quad C_{\mathrm{f}}=\frac{t_{\mathrm{w}}}{\frac{1}{2}u_{\mathrm{w}}^2\rho_{\mathrm{f}}}, \tag{14}$$

The reduced Sherwood number $-\phi'(0)$, skin-friction coefficient $K=0$, and the reduced Nusselt number $-\theta(0)$ are demarcated as

$$-\theta'(0) = \frac{Nu_x}{\sqrt{\frac{m+1}{2}Re}}, \quad -\phi'(0) = \frac{Sh_x}{\sqrt{\frac{m+1}{2}Re}}, \quad C_{fx} = \frac{C_f}{2}\sqrt{\frac{2}{m+1}Re}, \tag{15}$$

where $Re_x = \frac{u_w(x)x}{\nu}$ is the local Reynolds number

Results and discussion

The numerical outcomes of transformed nonlinear ordinary differential Eqs. (8)–(10) with boundary conditions (13) are elucidated via Keller-box method. For numerical result of physical parameters of our concern including *Nb* (Brownian motion parameter), *Nt* (thermophoresis parameter), *R* (Chemical reaction constraint), *M* (magnetic factor), *Gr* (local Grashof number), heat generation or absorption bound λ_1, *Gc* (local modified Grashof number), γ (inclination parameter), β (Casson fluid parameter), *Pr* (Prandtl number), *Le* (Lewis number), and *S* (suction or injection parameter), table and different figures are arranged. In Table 1, in the absence of *Gr*, *Gc*, *R*, *M*, *S*, and λ_1, with $\gamma = 90^o$ when Casson constraint $\beta \to \infty$ outcomes for reduced Sherwood number $-\phi'(0)$, reduced Nusselt number $-\theta'(0)$, are equated with the existing outcomes of Khan and Pop [41]. The effects of $-\theta'(0), -\phi'(0)$, and $C_{fx}(0)$ against different values of involved physical parameters *Nb*, β, *Nt*, *R*, *M*, λ_1, *Gr*, *Gc*, γ, *Pr*, *Le*, and *S* are presented in Table 2. It is noted that $-\theta'(0)$ decreases for increasing the values of *Nb*, *Nt*, $\lambda 1$, *Gr*, *Le*, *Gc*, and for decreasing values of *S* whereas, increased by enhancing the numerical values of $\beta, M, \gamma, Pr, m, R, S$. Moreover, it is observed that $-\phi'(0)$ enhanced with the larger values of M, m, β, R, Nt, and for small values of *S*. Whereas, decreases for cumulative the values of *Nb*, *Le*, λ_1, *Gr*, γ, *Gc*, and *S*. On the other hand, $C_{fx}(0)$ surges with the increasing values of *Nb*, *Le*, *M*, *m*, β, λ_1, γ, and for large values of *S*. Moreover, decreases with the increasing values of *Nt*, *Gr*, *Gc*, *Pr*, *R*, and for small values of *S*. Figure 2 portrays the velocity outline retards as we upturn the magnetic field constraint *M*. The logic behind is that magnetic field produces Lorentz force, by means slow down speed of the liquid. Moreover, similar result of velocity profile recovered by Jafar et al. [42]. Moreover, the velocity profile and nonlinear factor *m* have inverse relation see Fig. 3. The effects of suction parameter *S* on the velocity profile are shown in Fig. 4. It is perceived that the velocity profile decline by growing *S* parameter signifying the normal fact that suction steadies the boundary layer development due to which the creation of highest in the velocity outline also drops. The outcome of Casson constraint on velocity factor is presented in Fig. 5. It is detected that for different values of Casson parameter

Table 1 Contrast of the reduced Nusselt number $-\theta'(0)$ and the reduced Sherwood number $-\phi'(0)$ with $M, S, R, \lambda_1, Gr, Gc = 0$, $Pr = Le = 10$, $m = 1$ and $\gamma = 90°$ when $\beta \to \infty$

Nb	*Nt*	Khan and Pop [33]		Current outcomes	
		$-\theta'(0)$	$-\phi'(0)$	$-\theta'(0)$	$-\phi'(0)$
0.1	0.1	0.9524	2.1294	0.9524	2.1294
0.2	0.2	0.3654	2.5152	0.3654	2.5152
0.3	0.3	0.1355	2.6088	0.1355	2.6088
0.4	0.4	0.0495	2.6038	0.0495	2.6038
0.5	0.5	0.0179	2.5731	0.0179	2.5731

Table 2 Values of $-\theta'(0)$, $-\phi'(0)$ and $C_{fx}(0)$

Nb	*Nt*	*Pr*	*Le*	*M*	*m*	β	*R*	λ_1	*Gr*	*Gc*	*S*	γ	$-\theta'(0)$	$-\phi'(0)$	$C_{fx}(0)$
0.1	0.1	6.5	5.0	0.1	0.5	1.0	1.0	0.1	0.1	0.9	0.1	45°	1.7662	2.4211	0.3700
0.3	0.1	6.5	5.0	0.1	0.5	1.0	1.0	0.1	0.1	0.9	0.1	45°	1.1359	0.7801	0.4449
0.1	**0.3**	6.5	5.0	0.1	0.5	1.0	1.0	0.1	0.1	0.9	0.1	45°	1.4241	5.3833	0.1913
0.1	0.1	**10.0**	5.0	0.1	0.5	1.0	1.0	0.1	0.1	0.9	0.1	45°	2.2744	2.8943	0.3678
0.1	0.1	6.5	**10.0**	0.1	0.5	1.0	1.0	0.1	0.1	0.9	0.1	45°	1.4129	1.6403	0.4807
0.1	0.1	6.5	5.0	**0.5**	0.5	1.0	1.0	0.1	0.1	0.9	0.1	45°	1.8477	3.0037	0.5218
0.1	0.1	6.5	5.0	0.1	**1.5**	1.0	1.0	0.1	0.1	0.9	0.1	45°	1.8535	3.0828	0.5877
0.1	0.1	6.5	5.0	0.1	0.5	**5.0**	1.0	0.1	0.1	0.9	0.1	45°	1.8161	2.7219	0.3763
0.1	0.1	6.5	5.0	0.1	0.5	1.0	**2.0**	0.1	0.1	0.9	0.1	45°	2.0826	4.2966	0.2952
0.1	0.1	6.5	5.0	0.1	0.5	1.0	1.0	**0.3**	0.1	0.9	0.1	45°	1.3563	2.0224	0.3723
0.1	0.1	6.5	5.0	0.1	0.5	1.0	1.0	0.1	**1.0**	0.9	0.1	45°	1.7530	2.2727	0.2527
0.1	0.1	6.5	5.0	0.1	0.5	1.0	1.0	0.1	0.1	**2.0**	0.1	45°	1.7070	1.8359	0.0642
0.1	0.1	6.5	5.0	0.1	0.5	1.0	1.0	0.1	0.1	0.9	**0.3**	45°	2.3168	1.6795	0.5018
0.1	0.1	6.5	5.0	0.1	0.5	1.0	1.0	0.1	0.1	1.0	**0.0**	45°	1.5260	2.8454	0.2924
0.1	0.1	6.5	5.0	0.1	0.5	1.0	1.0	0.1	0.1	1.0	0.1	**60°**	1.7970	2.6672	0.4567

Bold indicates local modified Grashof number

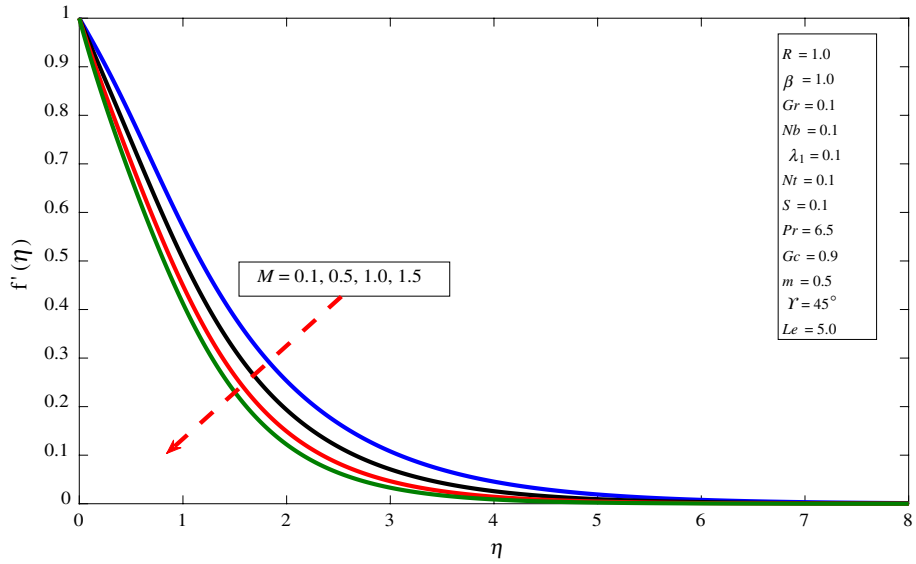

Fig. 2 Velocity profile for several values of M

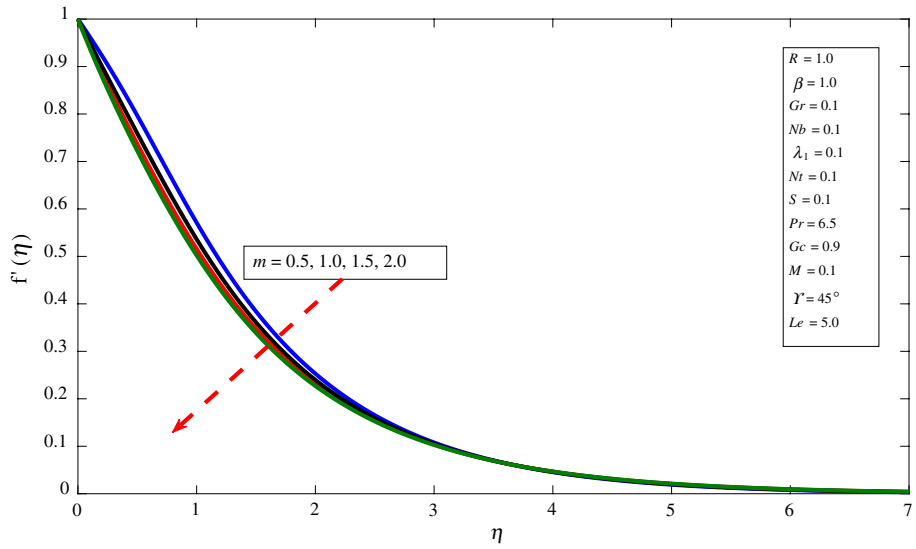

Fig. 3 Velocity profile for several values of m

velocity profile decreases. The cause overdue this behavior is that by growing the values of Casson parameter β increases the fluid viscosity i.e., falling the yield stress. Therefore, the momentum boundary layer thickness reduces. Figure 6 indicates that the velocity outline increases by enhancing local modified Grashof number. It is pragmatic that the velocity profile rises by improving the buoyancy limit.

Figure 7 indicates that the velocity profile diminishes with increment in inclination parameter γ. This is because of enhancing the value of inclination; decrease the strength of the bouncy force by a factor $\cos\gamma$ because of the thermal variation. Also, we found impact of bouncy force (which is highest for $\gamma = 0$) exceeds the main stream velocity. The temperature profile increases with the improvement in Brownian motion shown in Fig. 8. Moreover, contrary style is seen beside the concentration outline in Fig. 9. Substantially, the enlargement in Brownian movement factor supports to heat up the boundary layer due to which nanoparticles move from the extending surface to the liquid in rest. Therefore, the concentration nanoparticle moderates. Moreover, temperature and concentration profiles are increase for large values of Nt shown in Figs. 10 and 11. It is noted that the temperature and concentration contour upsurge in Figs. 12 and 13 by growing the values of heat

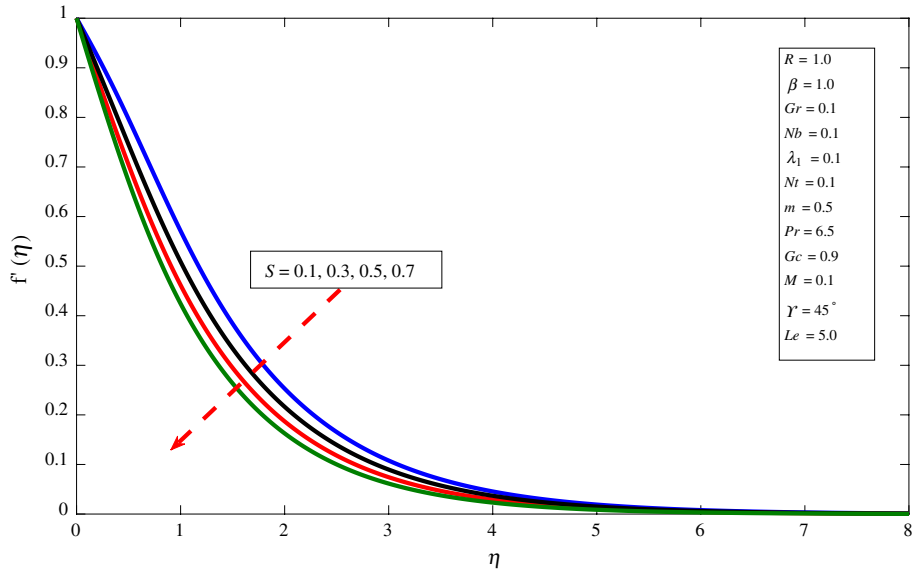

Fig. 4 Velocity profile for several values of S

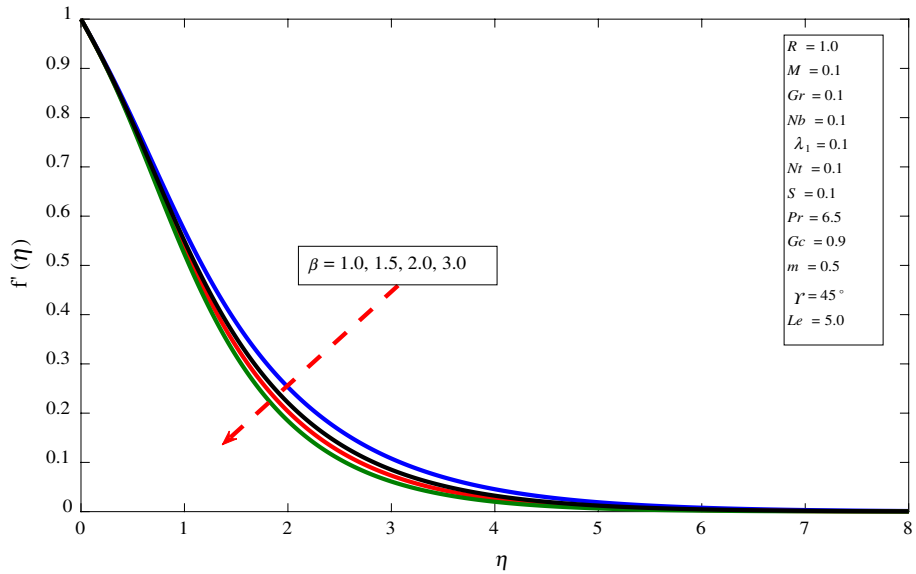

Fig. 5 velocity profile for several values of β

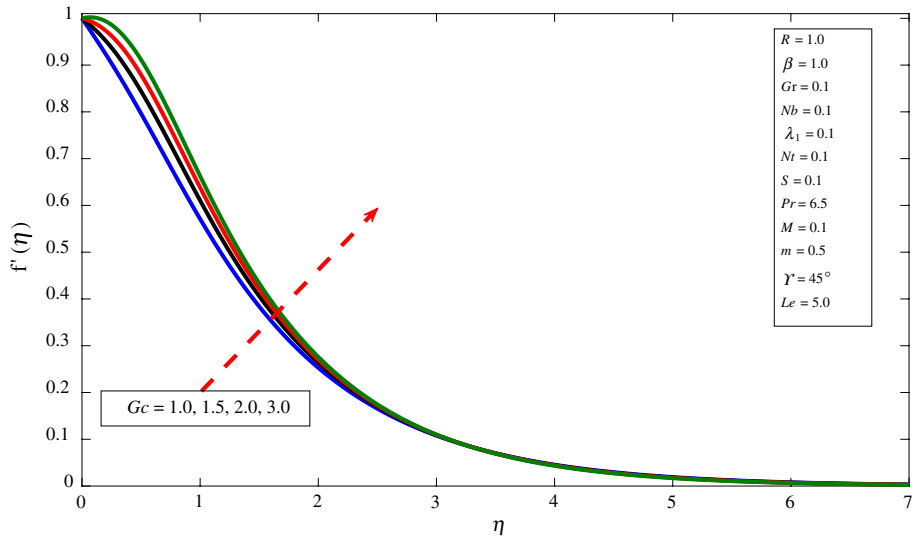

Fig. 6 Velocity profile for several values of *Gc*

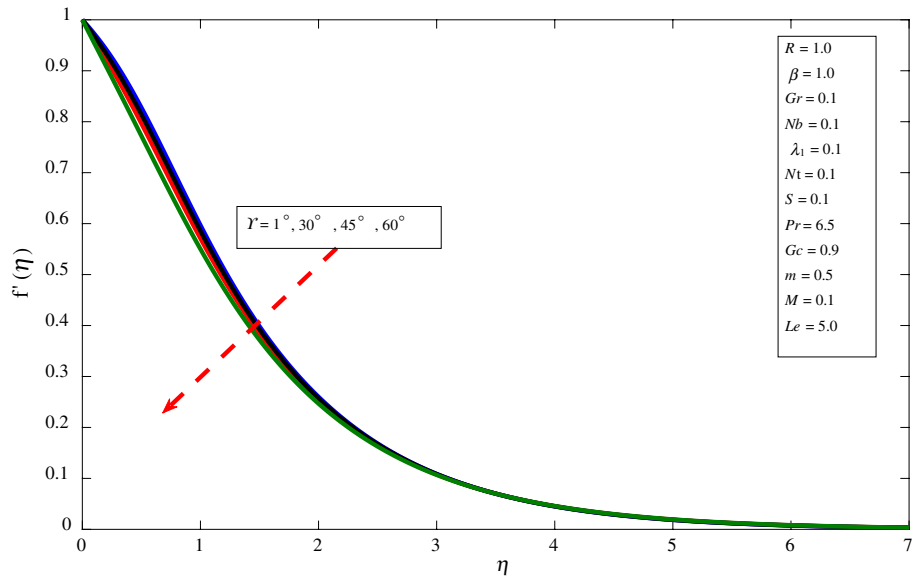

Fig. 7 Velocity profile for several values of γ

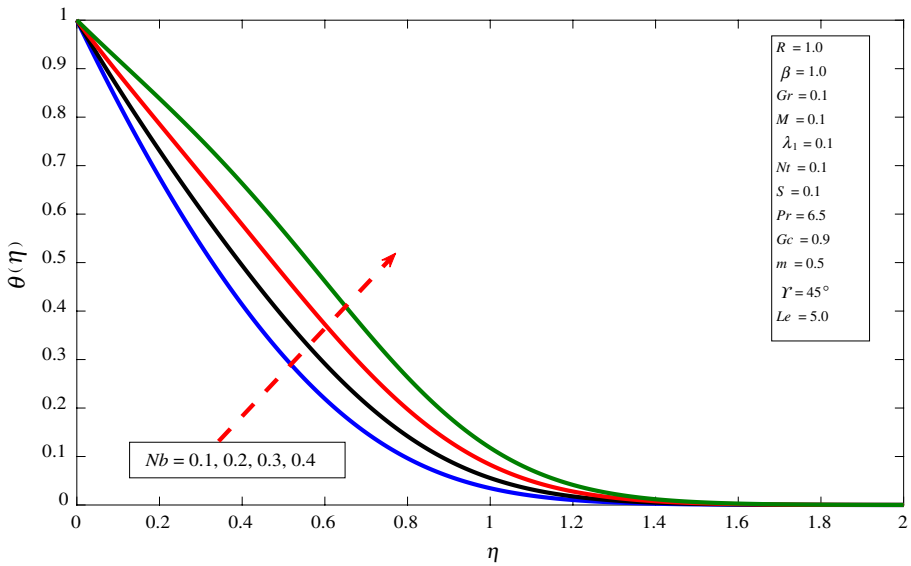

Fig. 8 Temperature profile for several values of *Nb*

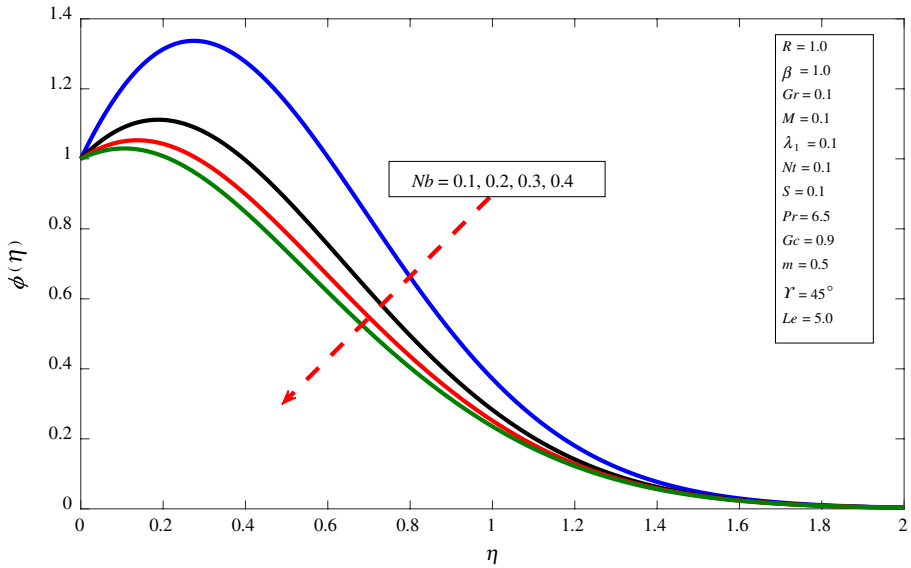

Fig. 9 Concentration profile for several values of *Nb*

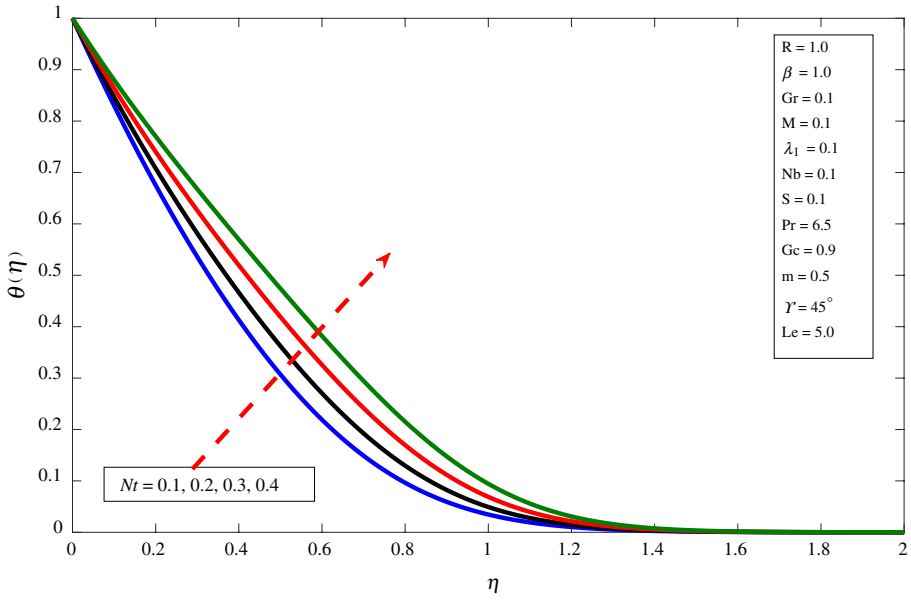

Fig. 10 Temperature profile for several values of *Nt*

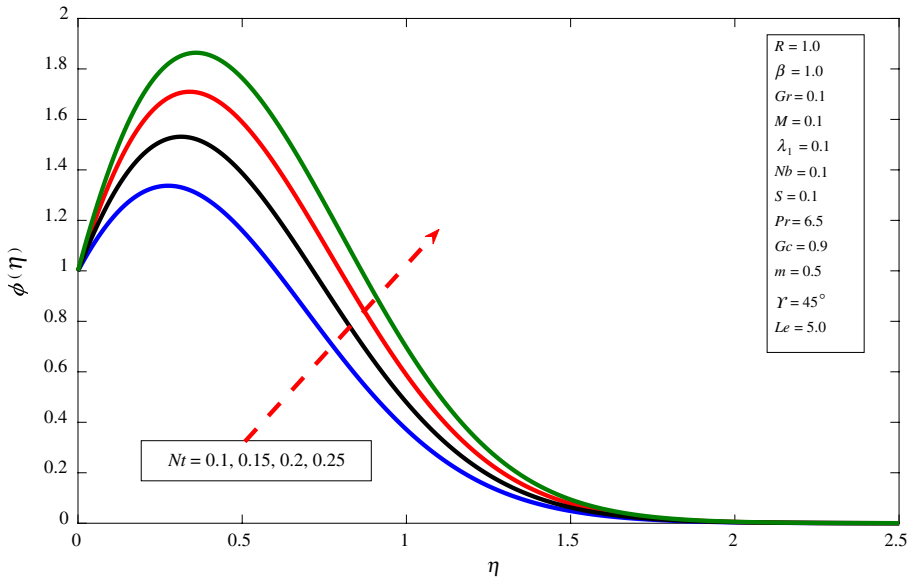

Fig. 11 Concentration profile for several values of *Nt*

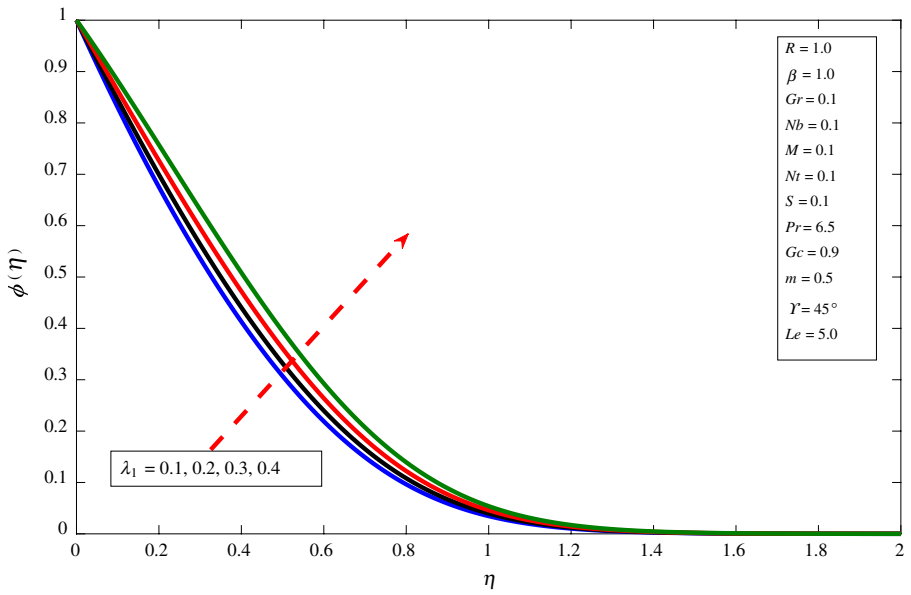

Fig. 12 Temperature profile for several values of λ_1

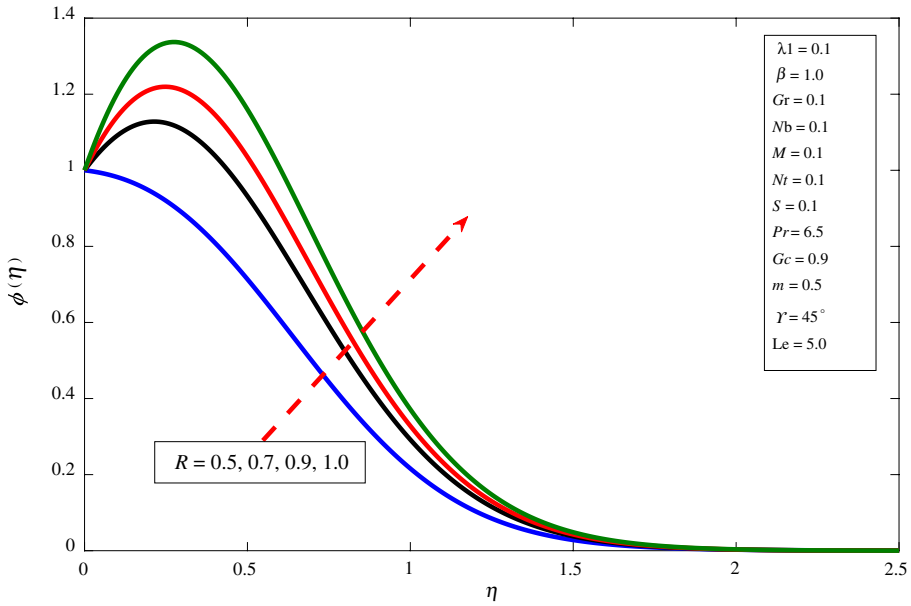

Fig. 13 Concentration profile for several value of R

generation constraint λ_1 and chemical reaction constraint R. The velocity of the liquid enhances by increasing the values of heat generation, due to which the temperature rises within the thermal boundary layer and heat breed in the flow region.

Conclusions

In current problem, we discussed the energy and species transport of Casson type nanofluid flow for nonlinear slanted stretching sheet. The impact of suction or injection and chemical reaction factors on energy and mass transfer rates are investigated numerically. The important conclusion points are the following.

- Increment in inclination factor diminishes velocity of the fluid.
- The velocity profile enhances with the growth of local Grashof number and local modified Grashof number.
- Energy and mass transport rates increase by increasing inclination.
- Casson parameter declines velocity of the fluid.
- Concentration profile improves with the increment in chemical reaction factor.

References

1. Rafique K, Anwar MI, Misiran M, Khan I, Alharbi SO, Thounthong P, Nisar KS. Numerical solution of Casson nanofluid flow over a non-linear inclined surface with Soret and Dufour effects by Keller-box method. Front Phys. 2019;7:39.
2. Anwar MI, Rafique K, Misiran M, Shehzad SA. Numerical study of hydrodynamic flow of a Casson nanomaterial past an inclined sheet under porous medium. Heat Transf Asian Res. 2020;49(1):307–34.
3. Imran MA, Shah NA, Rafique K, Sohail A, Ejaz S. General solutions of convective flows of MHD Casson fluid with slip and radiative heat transfer at the boundary. Comput Therm Sci Int J. 2017;9(1):1–11.
4. Ali Lund L, Omar Z, Khan I, Raza J, Bakouri M, Tlili I. Stability analysis of Darcy-Forchheimer flow of Casson type nanofluid over an exponential sheet: investigation of critical points. Symmetry. 2019;11(3):412.
5. Ali Lund L, Omar Z, Raza J, Khan I, Sherif ESM. Effects of Stefan blowing and slip conditions on unsteady MHD Casson nanofluid flow over an unsteady shrinking sheet: dual solutions. Symmetry. 2020;12(3):487.
6. Narender G, Govardhan K, Sarma GS. Magnetohydrodynamic stagnation point on a Casson nanofluid flow over a radially stretching sheet. Beilstein J Nanotechnol. 2020;11(1):1303–15.
7. Chary SB, Reddy KJ, Kashaiah K. Influence of thermal diffusion on MHD radiating flow in presence of Cu-nanoparticles, Casson fluid and angle of inclination. J Appl Math Comput Mech. 2020;19(2):43–57.
8. Ibrahim W, Anbessa T. Three-dimensional MHD mixed convection flow of Casson nanofluid with hall and ion slip effects. Math Probl Eng. 2020;2020:8656147.
9. Ahmad K, Halim SA, Hanouf Z. Variable viscosity of Casson fluid flow over a stretching sheet in porous media with Newtonian heating. J Inform Math Sci. 2018;10(1–2):359–70.
10. El-Aziz A, Afify AA. MHD Casson fluid flow over a stretching sheet with entropy generation analysis and Hall influence. Entropy. 2019;21(6):592.
11. Akgül A. Reproducing kernel Hilbert space method based on reproducing kernel functions for investigating boundary layer flow of a Powell-Eyring non-Newtonian fluid. J Taibah Univ Sci. 2019;13(1):858–63.
12. Baleanu D, Fernandez A, Akgül A. On a fractional operator combining proportional and classical differintegrals. Mathematics. 2020;8(3):360.
13. Akgül A. A novel method for a fractional derivative with non-local and non-singular kernel. Chaos Solitons Fractals. 2018;114:478–82.
14. Akgül EK. Solutions of the linear and nonlinear differential equations within the generalized fractional derivatives. Chaos Interdiscip J Nonlinear Sci. 2019;29(2):023108.
15. Arjmandfard A, Toghraie D, Mehmandoust B, Hashemian M, Karimipour A. Study the time evolution of nanofluid flow in a microchannel with various sizes of Fe nanoparticle using molecular dynamics simulation. Int Commun Heat Mass Transf. 2020;118:104874.
16. Zhang Y, Xie G, Karimipour A. Comprehensive analysis on the effect of asymmetric heat fluxes on microchannel slip flow and heat transfer via a lattice Boltzmann method. Int Commun Heat Mass Transf. 2020;118:104856.
17. Arjmandfard A, Toghraie D, Mehmandoust B, Hashemian M, Karimipour A. The study of atomic porosity effect on water/Fe nanofluid flow in a microchannel with a molecular dynamics method. J Mol Liq. 2020;317:114291.
18. Niknejadi M, Afrand M, Karimipour A, Shahsavar A, Isfahani AHM. An experimental study on the cooling efficiency of magnetite–water nanofluid in a twisted tube exposed to a rotating magnetic field. J Therm Anal Calorim. 2020;93:1–17.
19. Zhang Y, Xie G, Karimipour A, Sundén B. LBM modeling and analysis on microchannel slip flow and heat transfer under different heating conditions. Numer Heat Transf Part A Appl. 2020;78(5):159–79.
20. Jiang Y, Dehghan S, Karimipour A, Toghraie D, Li Z, Tlili I. Effect of copper nanoparticles on thermal behavior of water flow in a zig-zag nanochannel using molecular dynamics simulation. Int Commun Heat Mass Transf. 2020;116:104652.
21. Barnoon P, Toghraie D, Karimipour A. Application of rotating circular obstacles in improving ferrofluid heat transfer in an enclosure saturated with porous medium subjected to a magnetic field. J Therm Anal Calorim. 2020;48:1–23.
22. Wu H, Beni MH, Moradi I, Karimipour A, Kalbasi R, Rostami S. Heat transfer analysis of energy and exergy improvement in water-tube boiler in steam generation process. J Therm Anal Calorim. 2020;139(4):2791–9.
23. Eastman JA, Choi US, Li S, Thompson LJ, Lee S. Enhanced thermal conductivity through the development of nanofluids. MRS Online Proceedings Library Archive, 1996. p. 457.
24. Eastman JA, Choi US, Li S, Thompson LJ, Lee S. Nanophase and Nanocomposite Materials II 1997. vol. 457.
25. Buongiorno J. Convective transport in nanofluids. J Heat Transfer. 2006;128(3):240–50.
26. Sajjadi H, Mohammadifar H, Delouei AA. Investigation of the effect of the internal heating system position on heat transfer rate utilizing Cu/water nanofluid. J Therm Anal Calorim. 2019;353:1–20.
27. Gorjaei AR, Joda F, Khoshkhoo RH. Heat transfer and entropy generation of water–Fe_3O_4 nanofluid under magnetic field by Euler-Lagrange method. J Therm Anal Calorim. 2020;139(3):2023–34.
28. Sheikholeslami M, Gerdroodbary MB, Shafee A, Tlili I. Hybrid nanoparticles dispersion into water inside a porous wavy tank involving magnetic force. J Therm Anal Calorim. 2019;125:1–7.
29. Ghalambaz M, Doostani A, Izadpanahi E, Chamkha AJ. Conjugate natural convection flow of Ag–MgO/water hybrid nanofluid in a square cavity. J Therm Anal Calorim. 2020;139(3):2321–36.
30. Bazdar H, Toghraie D, Pourfattah F, Akbari OA, Nguyen HM, Asadi A. Numerical investigation of turbulent flow and heat transfer of nanofluid inside a wavy microchannel with different wavelengths. J Therm Anal Calorim. 2020;139(3):2365–80.
31. Rafique K, Anwar MI, Misiran M, Khan I, Sherif ESM. The implicit Keller box scheme for combined heat and mass transfer of brinkman-type micropolar nanofluid with Brownian motion

and thermophoretic effect over an inclined surface. Appl Sci. 2020;10(1):280.
32. Rafique K, Anwar MI, Misiran M, Khan I, Baleanu D, Nisar KS, Sherif E-S, Seikh AH. Hydromagnetic flow of micropolar nanofluid. Symmetry. 2020;12:251.
33. Bohra S. Heat and mass transfer over a three-dimensional inclined non-linear stretching sheet with convective boundary conditions. Indian J Pure Appl Phys. 2017;55(12):847–56.
34. Rafique K, Anwar MI, Misiran M. Keller-box study on Casson nano fluid flow over a slanted permeable surface with chemical reaction. Asian Res J Math. 2019;14:1–17.
35. Ellahi R, Zeeshan A, Hussain F, Abbas T. Two-phase couette flow of couple stress fluid with temperature dependent viscosity thermally affected by magnetized moving surface. Symmetry. 2019;11(5):647.
36. Reddy PBA. Magnetohydrodynamic flow of a Casson fluid over an exponentially inclined permeable stretching surface with thermal radiation and chemical reaction. Ain Shams Eng J. 2016;7(2):593–602.
37. Tlili I. Effects MHD and heat generation on mixed convection flow of Jeffrey fluid in microgravity environment over an inclined stretching sheet. Symmetry. 2019;11(3):438.
38. Ahmad S, Farooq M, Mir NA, Anjum A, Javed M. Magneto-hydrodynamic flow of squeezed fluid with binary chemical reaction and activation energy. J Cent South Univ. 2019;26(5):1362–73.
39. Rafique K, Anwar MI, Misiran M, Khan I, Seikh AH, Sherif ESM, Sooppy Nisar K. Keller-box simulation for the Buongiorno mathematical model of micropolar nanofluid flow over a nonlinear inclined surface. Processes. 2019;7(12):926.
40. Makinde OD, Olanrewaju PO. Buoyancy effects on thermal boundary layer over a vertical plate with a convective surface boundary condition. J Fluids Eng. 2010;132(4):044502-1.
41. Khan WA, Pop I. Boundary-layer flow of a nanofluid past a stretching sheet. Int J Heat Mass Transf. 2010;53(11–12):2477–83.
42. Jafar AB, Shafie S, Ullah I. MHD radiative nanofluid flow induced by a nonlinear stretching sheet in a porous medium. Heliyon. 2020;6(6):e04201.